Showcasing research from Prof. Antonio Monari, LPCT laboratory, Université de Lorraine and CNRS, Nancy, France, and Dr Virginie Lhiaubet-Vallet, ITQ Laboratory, Universitat Politècnica de València and CSIC, Valencia, Spain.

Photoinduced intersystem crossing in DNA oxidative lesions and epigenetic intermediates

New episode of the Trojan horse saga now available: 5-formyluracil and 5-formylcytosine triplet excited state population is established by theoretical calculations combined with spectroscopic experiments, which turns these lesions into potential intrinsic DNA photosensitizers.

As featured in:

See Antonio Francés-Monerris, Virginie Lhiaubet-Vallet, Antonio Monari *et al.*, *Chem. Commun.*, 2020, **56**, 4404.

ROYAL SOCIETY OF CHEMISTRY

rsc.li/chemcomm

Registered charity number: 207890

ChemComm

COMMUNICATION

View Article Online
View Journal | View Issue

Cite this: *Chem. Commun.*, 2020, **56**, 4404

Received 12th February 2020,
Accepted 27th March 2020

DOI: 10.1039/d0cc01132k

rsc.li/chemcomm

Photoinduced intersystem crossing in DNA oxidative lesions and epigenetic intermediates†

Antonio Francés-Monerris, *[ab] Mauricio Lineros-Rosa,[c] Miguel Angel Miranda, [c] Virginie Lhiaubet-Vallet *[c] and Antonio Monari *[a]

The propensity of 5-formyluracil and 5-formylcytosine, *i.e.* oxidative lesions and epigenetic intermediates, in acting as intrinsic DNA photosensitizers is unraveled by using a combination of molecular modeling, simulation and spectroscopy. Exploration of potential energy surfaces and non-adiabatic dynamics confirm a higher intersystem crossing rate for 5-formyluracil, whereas the kinetic models evidence different equilibria in the excited states for both compounds.

The accumulation of DNA lesions threatens the correct cell function and is associated to genomic instability, cell death, and carcinogenesis.[1–5] Ultraviolet light is known to trigger different photophysical and photochemical processes leading to the development of the so-called DNA photolesions,[3,6–8] widely recognized as one of the major causes of malignant skin cancer.[8] Understanding the subtle mechanisms leading to DNA lesions is fundamental to assure better public health protection strategies and therefore answer to a fundamental societal call. However, the photophysical and photochemical pathways leading to DNA lesion production are complex, and can be altered by the coupling with the complex inhomogeneous environment.[9,10] DNA photolesions can be obtained by direct UV light absorption or by photosensitization. Direct absorption of mainly UVB light leads to the dominant production of cyclobutane pyrimidine dimers (CPD), along with 6-4 photoproduct (64-PP) or 8-oxoguanine as minor components (see Fig. S1, ESI†).[8,11–15] Photosensitization proceeds through the initial absorption of UVA or visible light by a chromophore followed by different photochemical pathways.[16–23] It often requires the population of the triplet manifold of the photosensitizers, hence an efficient intersystem crossing (ISC) is a crucial prerequisite.[18,19,24–26] Recently, it has been proposed that the 64-PP DNA photolesion can by itself act as a photosensitizer leading to triplet energy transfer to nearby thymine, in what has been styled the "Trojan Horse" effect.[27–29] The same concept has been extended to oxidative lesions such as 5-formyluracil (**ForU**, see Fig. 1),[30,31] that is the principal product of pyrimidine oxidation and is potentially mutagenic.[32–34] The photosensitizing properties of **ForU** have been confirmed *in vitro* by UVA irradiation of supercoiled DNA,[31] whereas molecular modeling and simulation has evidenced the possibility of ISC and a feasible energy transfer to thymine.[30]

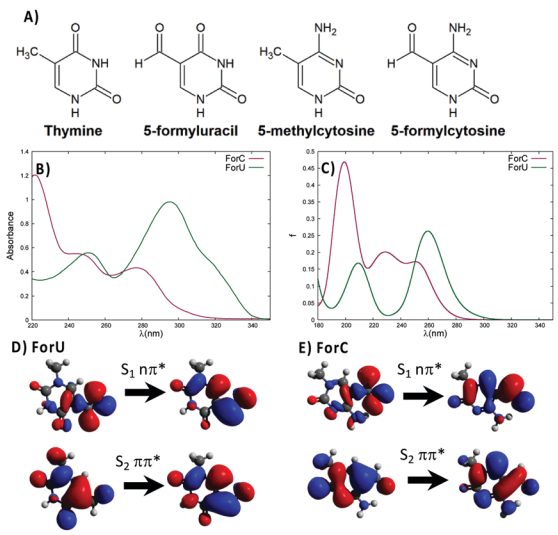

Fig. 1 Molecular formula of thymine, 5-formyluracil, 5-methylcytosine and 5-formylcytosine (A). Absorption spectra of **ForU** and **ForC** registered in PBS (B) and the corresponding TD-DFT simulated spectra in PCM (water solution) (C). NTOs for the first lowest transitions of **ForU** (D) and **ForC** (E).

[a] *Université de Lorraine and CNRS, LPCT UMR 7019, F-54000 Nancy, France. E-mail: antonio.frances@univ-lorraine.fr, antonio.monari@univ-lorraine.fr*
[b] *Departament de Química Física, Universitat de València, 46100 Burjassot, Spain*
[c] *Instituto Universitario Mixto de Tecnología Química UPV-CSIC, Universitat Politècnica de València, Avda de los Naranjos s/n, 46022 Valencia, Spain. E-mail: lvirgini@itq.upv.es*

† Electronic supplementary information (ESI) available: The simulated and experimental absorption spectrum for ForC and ForU in different solvents, Milli-Q absorption spectrum for ForU and ForC, experimental low temperature phosphorescence spectra, CAS active spaces, total standard deviation of the ensemble of the trajectories projected on the vibrational normal modes, representation of the most active vibrational normal modes, time evolution of the ring puckering parameters, computational and experimental methodology. See DOI: 10.1039/d0cc01132k

Molecular modeling studies[35] have suggested that 5-formylcytosine (**ForC**, Fig. 1), *i.e.* the oxidized form of the 5-methylcytosine, could lead to DNA photosensitization. **ForC** is an intermediate along the demethylation process of 5-methylcytosine essential for the epigenetic regulation of genes expression.[34,36–39] Moreover, formyl pyrimidine derivatives have been recognized as cancer biomarkers,[40] and recent biochemical evidence also notes the role of **ForC** as a stable epigenetic marker,[34,41] involved in chromatin remodeling.[42]

In this communication, in addition to the full characterization of the excited state manifold *via* the determination of the natural transition orbitals (NTO) and ϕ_S index,[43] we provide a comparison of the photophysical behavior of **ForU** and **ForC** *via* non-adiabatic molecular dynamics (NAMD)[44,45] through the SHARC 2.0 code.[45,46] The absorption spectra of **ForU** and **ForC** have been measured in different solvents, and simulated at time-dependent density functional theory (TD-DFT) level (Fig. 1 and ESI†), and are globally similar. In PBS, the absorption of **ForU** is red-shifted with respect to **ForC**, showing a maximum at around 300 nm and a tail reaching up to 340–350 nm (Fig. 1B). Conversely, the absorption maximum for **ForC** peaks at around 275 nm while the tail stops at 320–330 nm. The TD-DFT spectra (Fig. 1C) reproduce well the global band shapes both in the maximum and the tail regions, however, a systematic blue-shift is observed, most probably due to the use of polarizable continuum model (PCM) method to represent water solvation, hence neglecting specific solvent–chromophore interactions. NTO analysis (Fig. 1D and E)[47] shows that, for both nucleobases, the lowest transition giving rise to the long-wavelength tail is of $^1n\pi^*$ nature, while the S_2 state corresponds to $^1\pi\pi^*$ with electronic density reorganization delocalized over the full aromatic ring.

The gap between the two lowest-lying singlet states is larger for **ForU**, amounting to 1.1 eV at Franck–Condon geometry, while it decreases to 0.6 eV in the case of **ForC**. The calculated energy gaps between these two excited states are also in good agreement with the Milli-Q absorption spectra recorded in water (Fig. S2, ESI†) that yield a gap of 0.9 eV for **ForU** and 0.6 eV for **ForC**. Experimental and simulated spectra in different solvents (see ESI†) confirm that while the absorption of **ForC** is almost solvent independent, **ForU** exhibits slight solvatochromism.

The triplet excited states have been characterized from the low temperature phosphorescence spectra of the two oxidized nucleobases in ethanol (see Fig. S5, ESI†). Both compounds exhibit a shapeless emission, with a maximum at a λ_{em} of *ca.* 425 nm for **ForC**, whereas the phosphorescent emission of **ForU** is slightly red shifted and peaks at $\lambda_{em} = \sim 445$ nm (Table 1). Additionally, from the wavelength corresponding to the 20% of the emission, we have estimated the adiabatic energy levels of the lowest triplet state, that amount to 3.15 and 3.38 eV for **ForU** and **ForC**, respectively, indicating a lower triplet energy level for **ForU**.

To identify the emissive triplet states, the band origin and the band peak have been calculated with the TD-DFT method (see ESI†). The $^3n\pi^*$ state is identified as the most likely emissive state for **ForU**, whereas the $^3\pi\pi^*$ state is responsible of the **ForC** phosphorescence. This assignment is based on the good agreement between the calculated band maximum of the $^3n,\pi^*$ state and the experimental band peak (see Table 1), whereas the vertical emission wavelength of the $^3\pi\pi^*$ state of **ForU** is predicted at 513 nm, far from the 445 nm peak recorded experimentally, which matches much better the $^3n\pi^*$ vertical emission (427 nm). The CASPT2 method provides consistent results that support this interpretation (461 nm for $^3n\pi^*$ and 549 nm for $^3\pi\pi^*$ vertical emissions, respectively).

Even though the experimental and theoretical data presented in this work indicate that phosphorescence emerges from the $^3n\pi^*$ state, certain phosphorescence from the $^3\pi\pi^*$ state cannot be fully discarded also considering previous works on other modified nucleobases[48,49] and the energy degeneracy of both $^3n\pi^*$ and $^3\pi\pi^*$ states. Given the small oscillator strengths between n,π^* states and the ground state, longer phosphorescence lifetimes are expected for **ForU** with respect to **ForC**.

The PES of the two chromophores have been explored at CASPT2 and TD-DFT/B3LYP level, as reported in Fig. 2. In the case of **ForU**, the initially populated S_1 state ($^1n\pi^*$), evolves to its equilibrium geometry ($^1n\pi^*$ min) that also represents a singlet–triplet crossing (STC) region with the T_2 state ($^3\pi\pi^*$). An inversion of the diabatic triplet state ordering, compared with the Franck–Condon region, is evidenced at the **ForU** $^1n\pi^*$ minimum. Further exploration of the PES in the triplet manifold reveals the existence of two well defined minima for the $^3n\pi^*$ and $^3\pi\pi^*$ states separated by less than 0.2 eV in favor of the former, hence suggesting a possible coexistence of the two spectroscopic states. Note that both triplet minima can be considered as energetically degenerated independently of the specific theoretical method.

In contrast, **ForC** presents not only a larger singlet–triplet gap at the S_1 equilibrium geometry (about 0.3 eV), but also a lack of inversion between the $^3n\pi^*$ and the $^3\pi\pi^*$ states. SOC values are larger between $^1n\pi^*$ and $^3\pi\pi^*$ with respect to $^1n\pi^*$ and $^3n\pi^*$, providing a further argument in favor of a more efficient ISC for **ForU** than **ForC**. A good agreement between CASPT2 and B3LYP TD-DFT is observed validating the forthcoming NAMD performed at the TD-B3LYP level of theory. The time evolution of the population of the different states is reported in Fig. 3, confirming that, under the same simulation conditions, ISC is much more efficient for **ForU** than **ForC**.

Table 1 Experimental and computed values of the phosphorescence band origin and maxima for **ForU** and **ForC**. Energies are in eV and λ in nm (within parenthesis)

Compound	State	Band origin (TD-DFT)	Band origin (exp.)	Band maximum (TD-DFT)	Band maximum (exp.)
ForU	$^3n\pi^*$	3.23 (384)	3.15 (394)	2.99 (427)	~2.79 (445)
	$^3\pi\pi^*$	3.03 (409)		2.42 (513)	
ForC	$^3\pi\pi^*$	3.38 (367)	3.38 (367)	3.01 (411)	~2.92 (425)

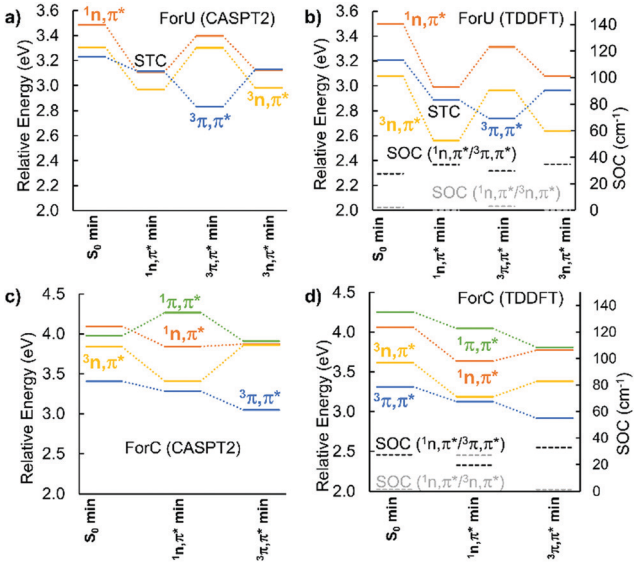

Fig. 2 Static profile positioning the most relevant critical points on the PES of **ForU** (panels A and B) and **ForC** (panels C and D). The calculated SOC between T_1 and T_2 with S_1 states are also reported at TD-DFT level. All energies are relative to the ground state at the S_0 min geometry. STC = singlet–triplet crossing.

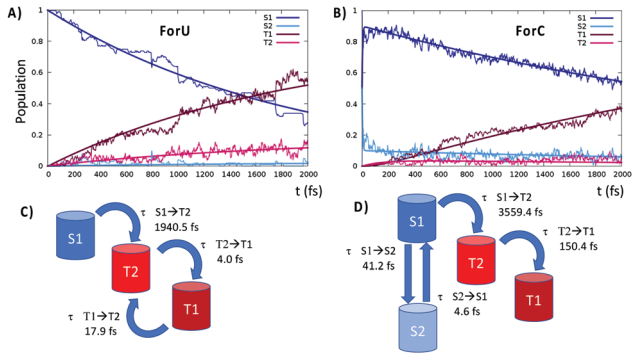

Fig. 3 Time evolution of the population of the different excited states for **ForU** (A) **ForC** (B). The curves obtained fitting the obtained population to the kinetic model for **ForU** (C) and **ForC** (D) are also shown, while the characteristic time constants are provided in panel (C) and (D).

While the absolute values of the ISC rates could be overestimated,[44] also due to gas-phase conditions, the tendencies between the two systems are correctly reproduced. Thus, after 2 ps the triplet manifold of **ForU** has a population exceeding 60%, whereas the population of the triplet state in **ForC** only reaches 40%. While in the case of **ForU**, a persistent population of T_2 is observed all along the NAMD, in **ForC** T_1 is the only significantly populated triplet state.

This difference can be better understood from the analysis of the hopping transitions between the states: in **ForU**, back and forward hops between the two lowest lying triplet states are observed, while in **ForC** only hops from T_2 to T_1 are present. Hence, in **ForU**, an equilibrium in the triplet state manifold is established leading to the persistent population of T_2, as was already observed in the case of benzophenone.[50] Analysis of the hopping transitions also allows to sketch the kinetic models reported in Fig. 3C and D for **ForU** and **ForC**, respectively.

The fitting of the population to the kinetic model provides the characteristic time constants for **ForU**, which are of about 1950 fs for the $S_1 \rightarrow T_2$ transition, representing the ISC rate limiting step, and of 4 and 17 fs for the $T_2 \rightarrow T_1$ and $T_1 \rightarrow T_2$ transitions, respectively. Instead, the kinetic model for **ForC** reveals a very rapid initial equilibrium in the singlet manifold with characteristic time constants of 41 and 5 fs for $S_1 \rightarrow S_2$ and $S_2 \rightarrow S_1$, respectively, followed by the rate limiting step $S_1 \rightarrow T_2$ transition that has a time constant of 3559 fs, *i.e.* almost double than the one of **ForU**. The subsequent internal conversion in the triplet manifold is fast and the time constant for the $T_2 \rightarrow T_1$ transition is of 150 fs.

Despite the different mechanism, and the different ISC rate limiting time, the behavior of the two oxidized nucleobases in terms of the vibrational normal modes leading to the triplet population are quite similar. The most active normal modes (Fig. 4) show that the displacements driving the ISC are related to ring breathing and deformation, coupled with some stretching and in plane bending of the aromatic ring substituents, their harmonic vibrational frequencies are comprised in the range 500–800 cm^{-1} for both systems. Out-of-plane deformations of the aromatic ring are totally absent, as confirmed by analysis of the ring puckering parameters (see ESI†) that only slightly deviates from the ideal planarity.

Our results confirm that **ForU** has the lowest triplet energy, of $^3n\pi^*$ nature, whereas the emissive state of **ForC** has $^3\pi\pi^*$ character. Both oxidized nucleobases can undergo ISC, and hence assure the first step of photosensitization, albeit with a different efficiency and with two different mechanisms, with **ForU** being much more efficient. The analysis of the non-adiabatic dynamic trajectories has confirmed that the normal modes driving the ISC are related to in-plane ring deformation. The absence of ring puckering modes, that could be hampered in the more confined DNA environment, suggests the maintaining of the favorable conditions for the triplet photosensitization in complex biological environments such as DNA double

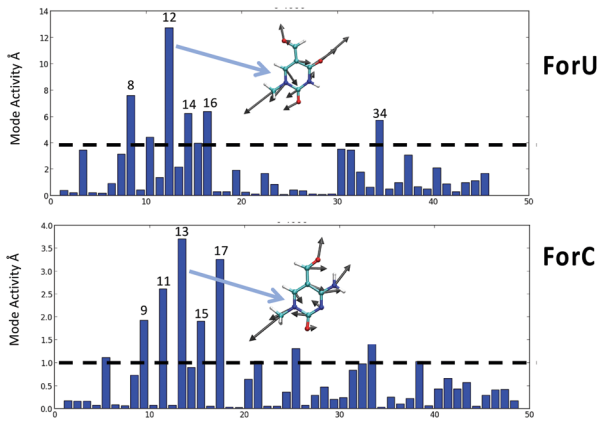

Fig. 4 Coherent activity of the vibrational normal modes for **ForU** (top) and **ForC** (bottom). The most active mode for **ForU** and **ForC** is also represented as an inset.

strands. Our work confirms the role of Trojan Horse bases, that could also involve biologically relevant epigenetic intermediates. In the future, we plan to extend this study by performing, on the one hand, non-adiabatic dynamics in the DNA environment to also evidence the triplet transfer to thymine, and on the other hand, to precisely measure the DNA photolesions induction by the two different chromophores.

Support from the Université de Lorraine, CNRS and Spanish Government (PGC2018-096684-B-I00) is kindly acknowledged. A. F.-M. is grateful to Generalitat Valenciana (CTQ2017-87054-C2-2-P) and the European Social Fund for a postdoctoral contract (APOSTD/2019/149), M. L.-R. acknowledges the Universitat Politècnica de València for the FPI grant. Calculations have been performed on the local LPCT computer center and on the Explor regional center in the framework of the project "Dancing under the light".

Conflicts of interest

There are no conflicts to declare.

References

1 R. Madabhushi, L. Pan and L. H. Tsai, *Neuron*, 2014, **83**, 266–282.
2 E. Sage, *Photochem. Photobiol.*, 1993, **57**, 163–174.
3 J. Cadet, E. Sage and T. Douki, *Mutat. Res., Fundam. Mol. Mech. Mutagen.*, 2005, **571**, 3–17.
4 G. T. Wondrak, *Skin stress response pathways: Environmental factors and molecular opportunities*, Springer, 2016.
5 J. Nakamura, E. Mutlu, V. Sharma, L. Collins, W. Bodnar, R. Yu, Y. Lai, B. Moeller, K. Lu and J. Swenberg, *DNA Repair*, 2014, **19**, 3–13.
6 L. Esposito, A. Banyasz, T. Douki, M. Perron, D. Markovitsi and R. Improta, *J. Am. Chem. Soc.*, 2014, **136**, 10838–10841.
7 H. Ikehata, T. Mori, Y. Kamei, T. Douki, J. Cadet and M. Yamamoto, *Photochem. Photobiol.*, 2020, **96**, 94–104.
8 J. Cadet and T. Douki, *Photochem. Photobiol. Sci.*, 2018, **17**, 1816–1841.
9 E. Dumont and A. Monari, *Front. Chem.*, 2015, **3**, 43.
10 J. Cadet and J. R. Wagner, *Cold Spring Harbor Perspect. Biol.*, 2013, **5**, a012559.
11 A. Banyasz, T. Douki, R. Improta, T. Gustavsson, D. Onidas, I. Vayá, M. Perron and D. Markovitsi, *J. Am. Chem. Soc.*, 2012, **134**, 14834–14845.
12 C. Rauer, J. J. Nogueira, P. Marquetand and L. González, *J. Am. Chem. Soc.*, 2016, **138**, 15911–15916.
13 H. Ikehata and T. Ono, *J. Radiat. Res.*, 2011, **52**, 115–125.
14 M. Gomez-Mendoza, A. Banyasz, T. Douki, D. Markovitsi and J. L. Ravanat, *J. Phys. Chem. Lett.*, 2016, **7**, 3945–3948.
15 A. Banyasz, L. Martínez-Fernández, C. Balty, M. Perron, T. Douki, R. Improta and D. Markovitsi, *J. Am. Chem. Soc.*, 2017, **139**, 10561–10568.
16 B. Epe, *Photochem. Photobiol. Sci.*, 2012, **11**, 98–106.
17 M. C. Cuquerella, V. Lhiaubet-Vallet, J. Cadet and M. A. Miranda, *Acc. Chem. Res.*, 2012, **45**, 1558–1570.
18 M. C. Cuquerella, V. Lhiaubet-Vallet, F. Bosca and M. A. Miranda, *Chem. Sci.*, 2011, **2**, 1219–1232.
19 V. Lhiaubet-Vallet and M. A. Miranda, in *CRC handbook of organic photochemistry and photobiology*, ed. F. Ghetti, A. G. Griesbeck and M. Oelgemöller, CRC Press, 2012, pp. 1541–1555.
20 J. Cadet, T. Douki and J. L. Ravanat, *Acc. Chem. Res.*, 2008, **41**, 1075–1083.
21 E. Dumont, R. Grüber, E. Bignon, C. Morell, Y. Moreau, A. Monari and J.-L. Ravanat, *Nucleic Acids Res.*, 2016, **44**, 56–62.
22 M. S. Baptista, J. Cadet, P. Di Mascio, A. A. Ghogare, A. Greer, M. R. Hamblin, C. Lorente, S. C. Nunez, M. S. Ribeiro, A. H. Thomas, M. Vignoni and T. M. Yoshimura, *Photochem. Photobiol.*, 2017, **93**, 912–919.
23 E. Dumont, M. Wibowo, D. Roca-Sanjuán, M. Garavelli, X. Assfeld and A. Monari, *J. Phys. Chem. Lett.*, 2015, **6**, 576–580.
24 É. Dumont and A. Monari, *J. Phys. Chem. B*, 2015, **119**, 410–419.
25 K. Hirakawa and T. Hirano, *Photochem. Photobiol.*, 2008, **84**, 202–208.
26 J. J. Nogueira, M. Oppel and L. González, *Angew. Chem., Int. Ed.*, 2015, **54**, 4375–4378.
27 V. Vendrell-Criado, G. M. Rodriguez-Muniz, M. C. Cuquerella, V. Lhiaubet-Vallet and M. A. Miranda, *Angew. Chem., Int. Ed.*, 2013, **52**, 6476–6479.
28 V. Vendrell-Criado, G. M. Rodríguez-Muñiz, V. Lhiaubet-Vallet, M. C. Cuquerella and M. A. Miranda, *ChemPhysChem*, 2016, **17**, 1979–1982.
29 E. Bignon, H. Gattuso, C. Morell, E. Dumont and A. Monari, *Chem. – Eur. J.*, 2015, **21**, 11509–11516.
30 A. Francés-Monerris, C. Hognon, M. A. Miranda, V. Lhiaubet-Vallet and A. Monari, *Phys. Chem. Chem. Phys.*, 2018, **20**, 25666–25675.
31 I. Aparici-Espert, G. Garcia-Lainez, I. Andreu, M. A. Miranda and V. Lhiaubet-Vallet, *ACS Chem. Biol.*, 2018, **13**, 542–547.
32 P. Liu, A. Burdzy and L. C. Sowers, *DNA Repair*, 2003, **2**, 199–210.
33 D. K. Rogstad, J. Heo, N. Vaidehi, W. A. Goddard, A. Burdzy and L. C. Sowers, *Biochemistry*, 2004, **43**, 5688–5697.
34 Y. Wang, X. Zhang, G. Zou, S. Peng, C. Liu and X. Zhou, *Acc. Chem. Res.*, 2019, **52**, 1016–1024.
35 J. Xing, Y. Ai, Y. Liu, J. Du, W. Chen, Z. Lu and X. Wang, *J. Phys. Chem. B*, 2018, **122**, 2704–2714.
36 V. López, A. F. Fernández and M. F. Fraga, *Ageing Res. Rev.*, 2017, **37**, 28–38.
37 A. Berson, R. Nativio, S. L. Berger and N. M. Bonini, *Trends Neurosci.*, 2018, **41**, 587–598.
38 C. Deans and K. A. Maggert, *Genetics*, 2015, **199**, 887–896.
39 C. Hognon, V. Besancenot, A. Gruez, S. Grandemange and A. Monari, *J. Phys. Chem. B*, 2019, **123**, 7365–7371.
40 Y. Tang, S. J. Zheng, C. B. Qi, Y. Q. Feng and B. F. Yuan, *Anal. Chem.*, 2015, **87**, 3445–3452.
41 M. Bachman, S. Uribe-Lewis, X. Yang, H. E. Burgess, M. Iurlaro, W. Reik, A. Murrell and S. Balasubramanian, *Nat. Chem. Biol.*, 2015, **11**, 555–557.
42 M. Iurlaro, G. Ficz, D. Oxley, E. A. Raiber, M. Bachman, M. J. Booth, S. Andrews, S. Balasubramanian and W. Reik, *Genome Biol.*, 2013, **14**, R119.
43 T. Etienne, X. Assfeld and A. Monari, *J. Chem. Theory Comput.*, 2014, **10**, 3896–3905.
44 R. Crespo-Otero and M. Barbatti, *Chem. Rev.*, 2018, **118**, 7026–7068.
45 S. Mai, P. Marquetand and L. González, *Wiley Interdiscip. Rev.: Comput. Mol. Sci.*, 2018, **8**, e1370.
46 S. Mai, P. Marquetand and L. González, *Int. J. Quantum Chem.*, 2015, **115**, 1215–1231.
47 R. L. Martin, *J. Chem. Phys.*, 2003, **118**, 4775–4777.
48 M. J. Janicki, R. Szabla, J. Šponer and R. W. Góra, *Chem. Phys.*, 2018, **515**, 502–508.
49 S. Mai, M. Pollum, L. Martínez-Fernández, N. Dunn, P. Marquetand, I. Corral, C. E. Crespo-Hernández and L. González, *Nat. Commun.*, 2016, **7**, 1–8.
50 M. Marazzi, S. Mai, D. Roca-Sanjuán, M. G. Delcey, R. Lindh, L. González and A. Monari, *J. Phys. Chem. Lett.*, 2016, **7**, 622–626.